J Mater Sci (2010) 45:1091–1099
DOI 10.1007/s10853-009-4051-1

Microstructure and tensile properties of metal injection molding Co–29Cr–6Mo–0.23C alloy

P. V. Muterlle · M. Zendron · M. Perina · R. Bardini · A. Molinari

Received: 2 April 2009 / Accepted: 18 November 2009 / Published online: 3 December 2009

Abstract The microstructure and tensile properties of a metal injection molding 0.23%C Co–Cr–Mo alloy (F75 alloy) were investigated. The as-sintered microstructure contains a significant amount of carbides, and is modified by solution annealing, the main effect being to reduce the amount of carbides. Ductility and ultimate tensile strength increase significantly, but yield strength decreases with solution annealing. Aging causes both intragranular and intergranular precipitation, which increases hardness and yield strength but decreases ductility excessively. In both as-sintered and solution-annealed conditions, the material displays noticeable work hardenability. By sintering at 1300 °C and solution annealing at 1220 °C, 440 MPa yield strength and 25% elongation at fracture are obtained.

Introduction

The mechanical properties of the Co–Cr–Mo–C castings depend on the carbon content, which promotes the precipitation of carbides at the grain boundary and in the interdendritic regions [1, 2]. Carbides increase hardness, yield stress, and wear resistance, but reduce ductility. On the other hand, a high carbon content increases the fluidity of the liquid alloy, improving castability. To improve ductility, carbides are dissolved in the metallic matrix by solution annealing [3, 4]. This treatment can be followed by aging to further modify the microstructure, both precipitating carbides more uniformly and modifying the matrix constitution through the transformation of austenite into martensite [5–7]. The effect of the microstructure on the mechanical properties has been studied by Vander Sande et al. [8].

As an alternative to casting, the Co–Cr–Mo-C alloys can be produced by metal injection molding (MIM) of prealloyed powders. The powders are mixed with a binder (around 50 vol%) to produce a feedstock having the proper rheological properties to be injected at a moderate temperature and pressure in a rigid die and to keep the shape once the injection pressure has been removed [9]. After debinding, parts are highly porous and are sintered at high temperature (1300–1380 °C) to obtain a full density. The carbon content of the commercially available powders varies in a broad range (0.05–0.35%).

In some previous works, relevant to a maximum carbon content of 0.15% [10–12], the effect of the sintering atmosphere composition was investigated. The presence of nitrogen enhances densification and strength, because of some nitrogenization occurring at high temperature. The mechanical properties are further improved by solution annealing and hot isostatic pressure.

A higher carbon content (0.3–0.35% C) promotes the formation of eutectic liquids which activate sintering; therefore, sintering temperature is lower than in the case of a low-carbon alloy [13]. The as-sintered microstructure is very different from the as-cast one; it contains quite large

P. V. Muterlle (✉) · A. Molinari
Dipartimento di Ingegneria dei Materiali e Tecnologia Industriali, Università di Trento, Mesiano 77, 38100 Trento, Italy
e-mail: palloma.muterlle@ing.unitn.it

A. Molinari
e-mail: alberto.molinari@ing.unitn.it

M. Zendron · M. Perina · R. Bardini
MIMEST, Viale Dante 300, 38057 Pergine Valsugana, Trento, Italy
e-mail: marianna.zendron@mimest.com

M. Perina
e-mail: matteo.perina@mimest.com

R. Bardini
e-mail: rudj.bardini@mimest.com

(several tenths of micrometers) equiaxed grains, with large eutectic cells and/or intergranular carbides, the amount of which depends on the carbon content.

In a previous work, the microstructure and the tensile properties of two alloys with extreme carbon contents (0.05% and 0.35%) were investigated [13]. While the low-carbon alloy has a good combination of strength and ductility in the as-sintered condition, the high-carbon alloy has to be solution annealed (SA) to obtain an acceptable ductility [13].

In this work, an alloy with an intermediate carbon content (0.23%C) was studied. Again, the microstructure was modified by heat treatment (solution annealing and aging) to study the phase transformations and their effect on mechanical properties. Tensile tests were carried out in all the conditions investigated, and the results were interpreted on the basis of the microstructural characteristics and on the deformation behavior deduced by the analysis of the fracture surfaces.

Experimental procedures

A prealloyed, gas-atomized Co–29Cr–6Mo (F75) powder with 0.23% carbon was used for the production of the specimens.

The powder was mixed with a proprietary binder (polyolefin based) to produce the feedstock. Test bars, according to ASTM E 8M-03—Standard Flat Unmachined Tension Test Specimen for Powder Metallurgy (P/M) Products, were injection molded and debinded by a two-step process (80% of the total binder content was dissolved in water, while the remaining 20% was removed by thermal decomposition). Thermal debinding was carried out in nitrogen atmosphere. The samples were sintered in vacuum furnace under the conditions reported in Table 1.

The sintered tensile bars were SA for 4 h at 1220 °C in a vacuum furnace, with argon backfilling and gas quenching in 8 bar nitrogen flux. Then, the samples were aged in a tubular furnace at 750 °C with Ar atmosphere for 3 and 20 h, and then air quenched.

The carbon content was measured by LECO CS125 after each heat treatment. Sintered density was determined by Archimedes' method on the as-sintered pieces.

Table 1 Sintering conditions

Carbon content (wt%)	Sintering conditions
F75 with 0.23%C (LT)	Sintering at 1300 °C, holding 1 h with N_2 backfilling, free cooling
F75 with 0.23%C (HT)	Sintering at 1350 °C, holding 1 h with N_2 backfilling, free cooling

The microstructure was investigated by light optical microscopy (LOM) and by environmental scanning electron microscopy (ESEM) before and after electrolytic etching with 94 mL distilled water, 4.5 mL HNO_3, and 1.5 mL H_2O_2 solution for 3 V and 4 s. The staining method, a chemical color etching with 1 part (20% $KMnO_4$ + 80% water) + 1 part (8% NaOH + 92% water) was carried out after electrolytic etching to distinguish the different types of carbides ($Cr_{23}C_6$ brown, Cr_7C_3 pale yellow to light tan, M_6C red, green, yellow, blue). Grain size was measured according to ASTM E112-96 standard.

The constitution of the metallic matrix (fcc/hcp phases) was investigated by X-ray diffractometry (XRD). The diffraction patterns were collected using a Cu-Kα source, and the experimental spectra were elaborated with the Rietveld method using the MAUD software (Materials Analysis Using Diffraction) [14, 15].

HV0.05 microhardness and HV30 hardness were measured. Tensile tests were carried out in an Instron machine at a strain rate of 0.1 s^{-1} and measuring strain with an axial extensometer with a gage length of 12.5 mm. Three specimens were tested for each material and microstructural condition. The fracture surfaces were investigated by ESEM.

Results

As-sintered materials

Density of the high-temperature (HT) material (8.18 g/cm^3, 98.7% of the theoretical density) is higher than that of the low-temperature (LT) material (7.55 g/cm^3, 91.1% of the theoretical density).

Figure 1a and b shows the microstructure of the materials sintered at the two temperatures.

It comprises the metallic matrix with an extensive precipitation of carbides confined in the grain boundary regions. On increasing the sintering temperature, the matrix grain size increases from 75 ± 16 μm up to 193 ± 25 μm. The LT material contains only lamellar "pearlite-type" eutectic carbides of the $Cr_{23}C_6$ type, as confirmed by the color metallographic etching. The HT material contains a second eutectic carbide, M_6C, which appears more compact in Fig. 1b. The $Cr_{23}C_6$ carbides are the product of the slow eutectic solidification of a liquid phase [3]. M_6C can both precipitate directly from the fcc solid solution and form as a product of the transformation on heating of $M_{23}C_6$ [2, 16].

The two types of eutectic carbides are better resolved at the ESEM, as shown by Fig. 2a and b, relevant to the low- and high-temperature sintered materials, respectively. Moreover, the ESEM micrographs show the grain boundary precipitation of sigma phase. The formation of this

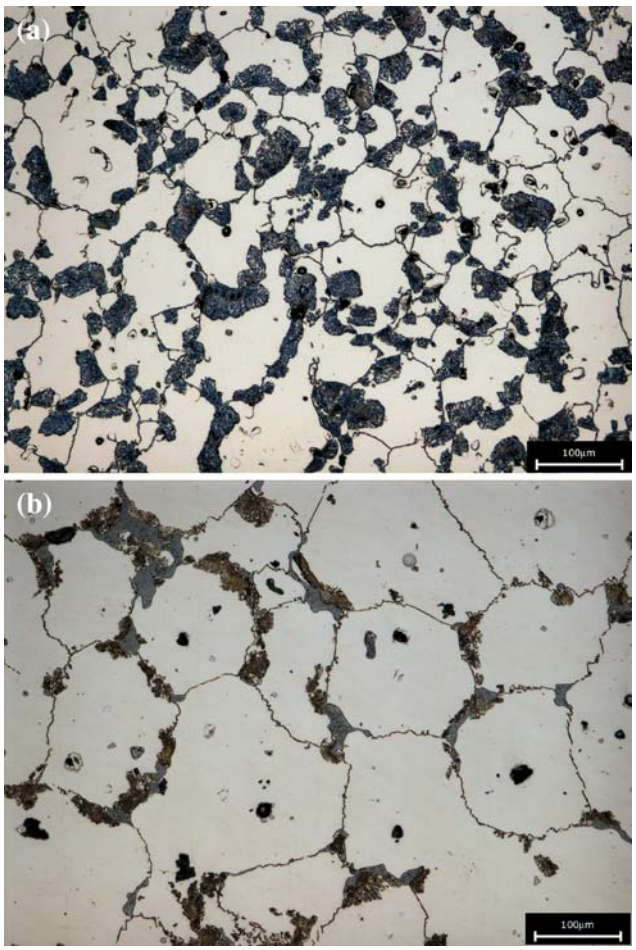

Fig. 1 Optical micrographs of as-sintered materials. **a** LT. **b** HT

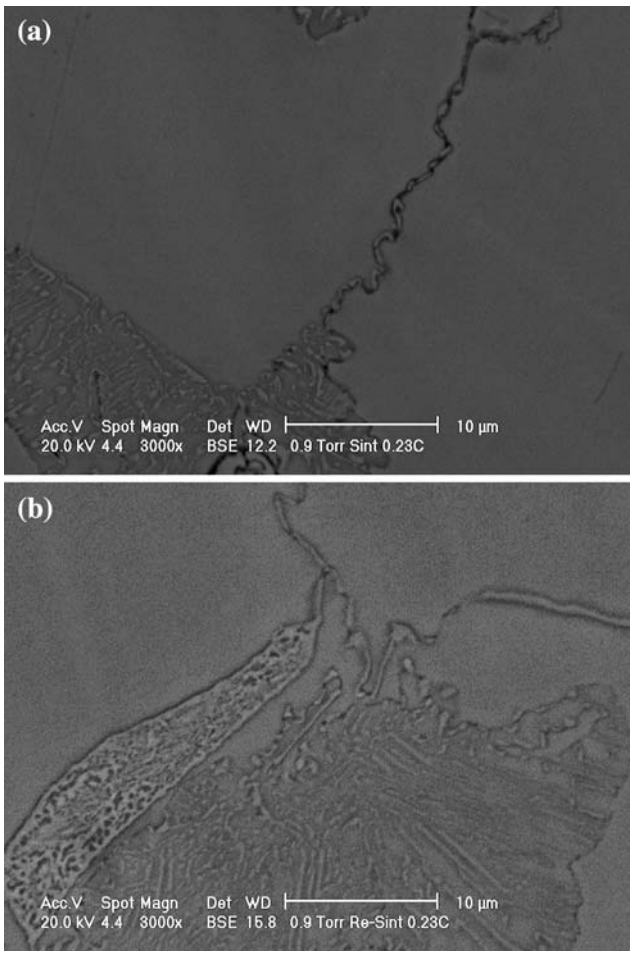

Fig. 2 ESEM micrographs of as-sintered materials. **a** LT. **b** HT

constituent was detected by Signorelli, in conjunction with, or subsequent to, $M_{23}C_6$ precipitation [2]. According to Shortsleeve and Nicholson [17], the precipitation of carbides promotes the formation of sigma phase, and then a large quantity of carbides enhances the probability of the precipitation of sigma phase.

Solution-annealed materials

Figure 3 shows the microstructure of the SA materials.

All the carbides and sigma phase are fully solubilized in the metallic matrix of the LT material, while some small spheroidized $Cr_{23}C_6$ particles are still present at the grain boundary of the HT alloy. These particles are shown in Fig. 4, and are the product of breaking-up and spheroidization of the lamellar "pearlite-like" eutectic carbides [2]. Grain size increases up to 90 ± 13 µm in the material sintered at lower temperature, while it remains almost unchanged in the other one, because of the grain boundary pinning exerted by the residual carbides.

Aged materials

Figures 5 and 6 show the microstructure of the aged materials.

Aging promotes an intragranular star-shape (Widmanstätten type) precipitation and the formation of a fine constituent (very closely packed lamellae), which nucleates at the grain boundary and grows inside grains. The amount of these precipitates increases with the aging time.

The Widmanstätten precipitates are $M_{23}C_6$ particles [2, 7, 18, 19]. Solution annealing and aging are then effective in promoting the formation of a homogeneous dispersion of carbides in the metallic matrix from the highly segregated microstructure of the as-sintered materials. The fine lamellar constituent is described by Rajan [18, 19]. For short aging time, an hcp phase containing some carbides nucleates at the grain boundary (hcp_1). On increasing aging time, it evolves to the hcp_2, which differs from hcp_1 for the lack of any crystallographic relationships with the parent phases and for the lower fault density. This evolution is coupled to an abundant precipitation of carbides.

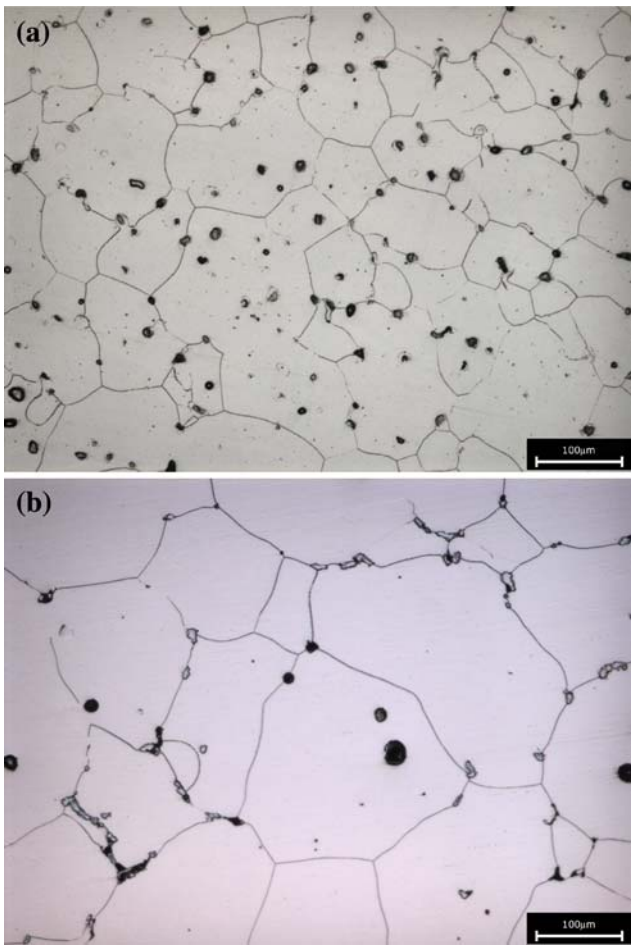

Fig. 3 Optical micrographs of SA materials. **a** LT. **b** HT

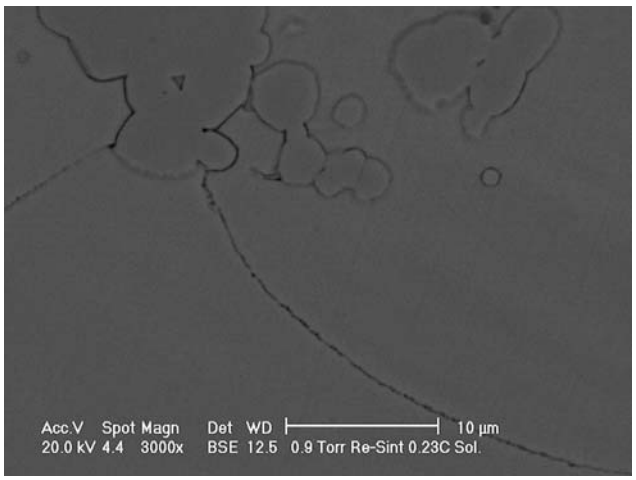

Fig. 4 ESEM micrographs of SA HT material

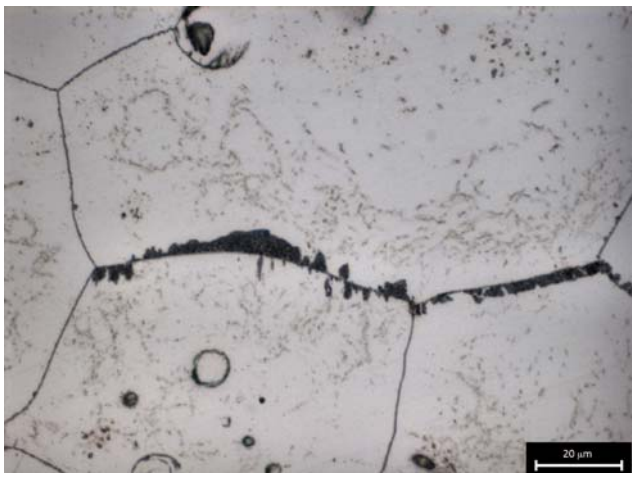

Fig. 5 Optical micrographs of LT material aged 3 h

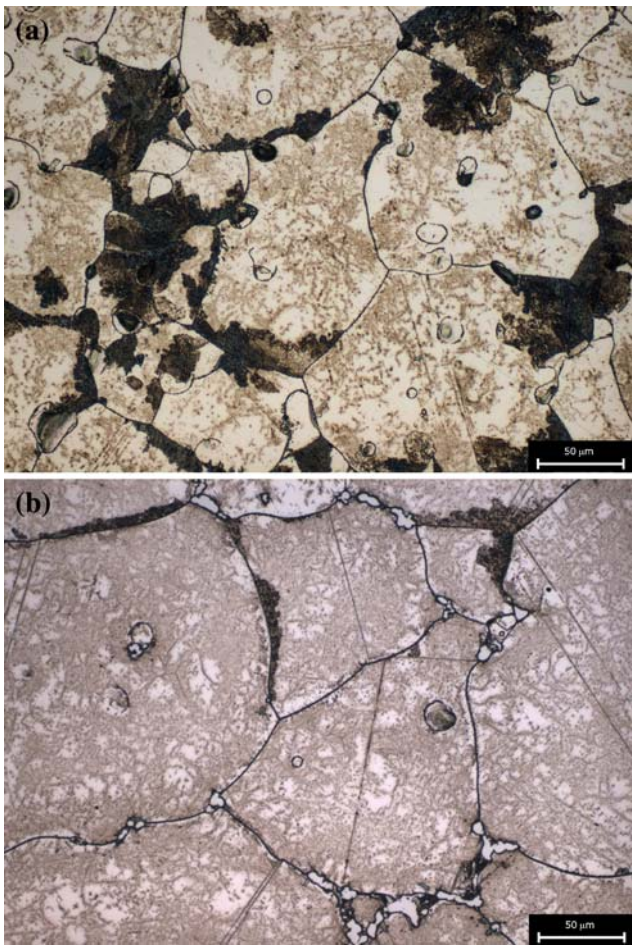

Fig. 6 Optical micrographs of LT (**a**) and HT (**b**) materials aged 20 h

Grain size does not change with aging. The LT material presents a higher quantity of grain boundary hcp constituents than the other one, likely because of the smaller grain size (larger grain boundary surface area which enhances nucleation) and the partial solubilization of the as-sintered carbides in the HT material. It also shows a less amount of Widmanstätten carbides, because of the concurrent carbide precipitation coupled to hcp phases.

XRD analyses

Figure 7 shows the XRD spectra of the two materials in the as-sintered and SA conditions. In Table 2, the results of the quantitative XRD analyses are reported.

The matrix of the two as-sintered materials consists of both fcc and hcp phases, with the latter prevailing. Despite the different amounts of carbides, the percentage of fcc and hcp phases is the same. In the LT material, fcc phase is stabilized by the residual interstitial carbon. The HT material contains the Mo-rich M_6C carbide (which is absent in LT), and has a significantly larger grain size. The precipitation of M_6C depletes the matrix in Mo; since this element stabilizes hcp phase [20], the reduction of its content as substitutional element in fcc phase effectively increases its stability, in comparison to LT material. Grain growth, on the other side, promotes the fcc to hcp transformation [20]. The two effects are then balanced, and the amount of hcp in the as-sintered materials does not change with the sintering temperature. After solution annealing, the quantity of fcc phase increases in the LT material. This is due to the complete solubilization of carbides, which increases the amount of interstitial carbon. The fcc phase is then stabilized against the transformation in hcp on quenching. In HT material, solution annealing dissolves preferentially the M_6C particles, leading to an increase in the Mo content of the fcc phase. Consequently, the transformation in hcp in quenching is enhanced, and the amount of fcc phase decreases with heat treatment.

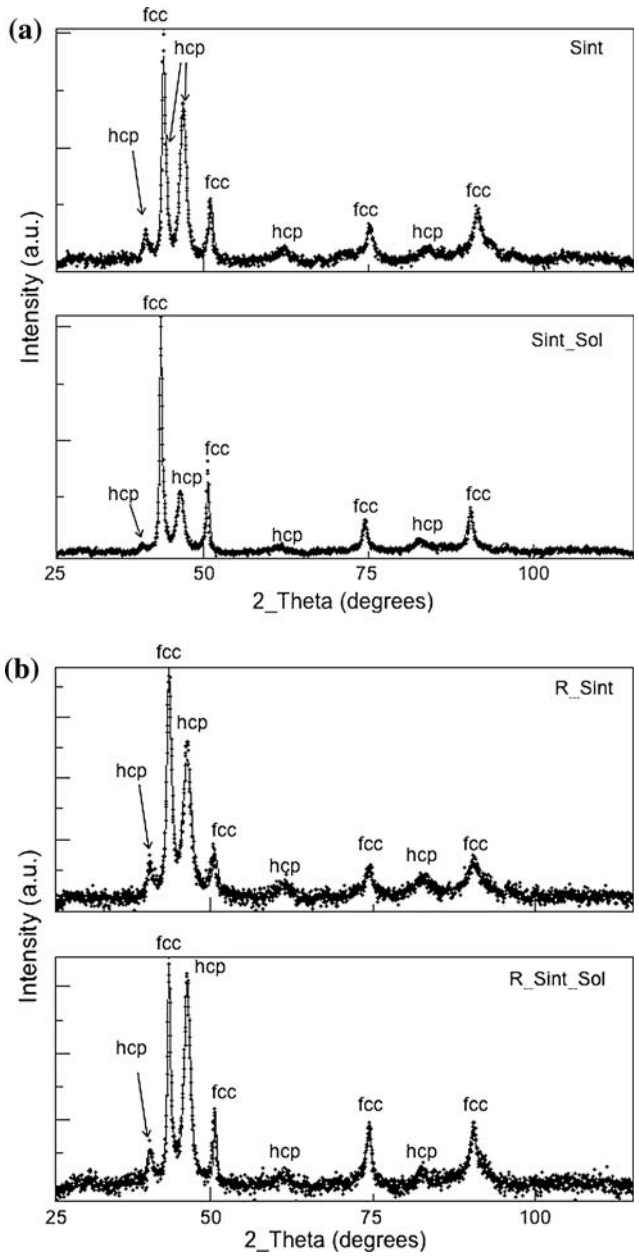

Fig. 7 XRD spectra of LT (**a**) and HT (**b**) materials

Table 2 XRD analyses

Samples	Constitution of the metallic matrix	
	% fcc	% hcp
LT		
As sintered	42 ± 1.2	58 ± 1.2
Sintered + SA	61 ± 1.2	39 ± 1.2
HT		
As sintered	43 ± 1.5	57 ± 1.5
Sintered + SA	33 ± 1.5	67 ± 1.5

XRD analyses were not carried out on aged materials because of their less interest for mechanical properties as described in the next section.

Mechanical properties

The results of hardness and microhardness measurements, as well as tensile tests, are presented in Table 3.

Hardness of the LT materials decreases with solution annealing because of grain growth and dissolution of carbides. These two effects prevail on the solution hardening of the metallic matrix (indicated by microhardness) provided by the enrichment in alloy elements. Contrarily, solution hardening of the matrix causes a slight increase in hardness of the HT material, since solution annealing does not eliminate all carbides and does not cause grain growth. On aging, hardness increases because of the intragranular precipitation of the Widmanstätten carbides (as demonstrated by the matrix microhardness) and of the grain boundary lamellar constituent. The lower density of the LT material accounts for the lower hardness, with respect to that sintered at higher temperature. The differences in microhardness between the two materials in the same treatment conditions are quite small (within the scatter

Table 3 Hardness, microhardness, and tensile properties of the investigated materials

Samples	Microhardness (HV0.05)	Hardness (HV30)	Tensile test		
			YS (MPa)	UTS (MPa)	Elongation %
LT					
As sintered	344 ± 26	246 ± 8	482 ± 11	789 ± 25	13 ± 3
Sintered + SA	369 ± 16	215 ± 4	442 ± 20	811 ± 29	25 ± 1
Sintered + SA + Ag3	389 ± 26	243 ± 2	511 ± 13	765 ± 3	10 ± 1
Sintered + SA + Ag20	401 ± 37	304 ± 7	730 ± 25	913 ± 1	2 ± 0.5
HT					
As sintered	365 ± 12	282 ± 8	426 ± 2	695 ± 8	10 ± 1
Sintered + SA	375 ± 19	313 ± 16	440 ± 9	763 ± 6	18 ± 1
Sintered + SA + Ag3	402 ± 13	389 ± 14	602 ± 27	780 ± 6	4 ± 1
Sintered + SA + Ag20	521 ± 38	480 ± 8	820 ± 3.0	962 ± 7	2 ± 0.5
Co–28Cr–6Mo SA (<0.1%C—MIM) [11]			>350	>600	>16
ASTM F75 (Cast)			>450	>655	>8
ASTM F1537 (Wrought)			>520	>900	>20

band), apart after 20 h aging, because of the different amount of Widmanstätten carbides.

As far as tensile properties of as-sintered materials are concerned, both strength and ductility of that LT material are surprisingly better than those of the HT material, despite the lower density. The higher yield stress may be correlated to the smaller grain size, according to the Hall–Petch relation. Figure 8 shows the fracture surface of the two as-sintered materials.

Fracture is fully intergranular and associated with the presence of carbides and sigma phase which cause strain localization and favor the nucleation and propagation of cracks [4].

Solution annealing causes a slight decrease (LT) and a slight increase (HT) in yield strength (YS), according to the effect on hardness. Because of the increased plasticity of the materials, ductility and ultimate tensile strength (UTS) increase. Again, the material sintered at lower temperature has better mechanical properties than the high temperature one. The different grain size and the residual grain boundary carbides are responsible for this difference. After solution annealing, the mechanical properties of the two materials exceed the requirements of ASTM F75 and the values of MIM CoCrMo alloys with less than 0.1%C and SA. The requirements for ASTM F1537 were not achieved.

The fracture surface of the SA materials (Fig. 9) gives evidence of the improved ductility in respect to the as-sintered ones. Fracture involves the cobalt matrix, which shows striations similar to deformation bands in the regions between the zones of intense shear. Only in the material sintered at the higher temperature (Fig. 9b), a brittle morphology is visible, attributable to residual grain boundary carbides. The low amount of carbides and the absence in the LT material allow deformation to propagate through the metallic matrix.

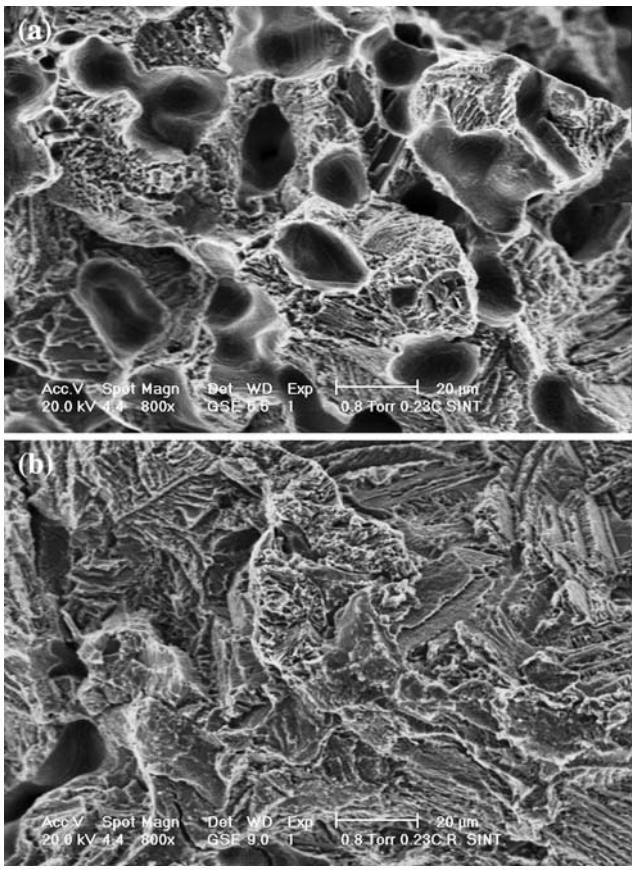

Fig. 8 Fracture surface for as-sintered materials. **a** LT. **b** HT

In aged specimens, strength increases, but ductility strongly decreases (Table 3), because of the extensive

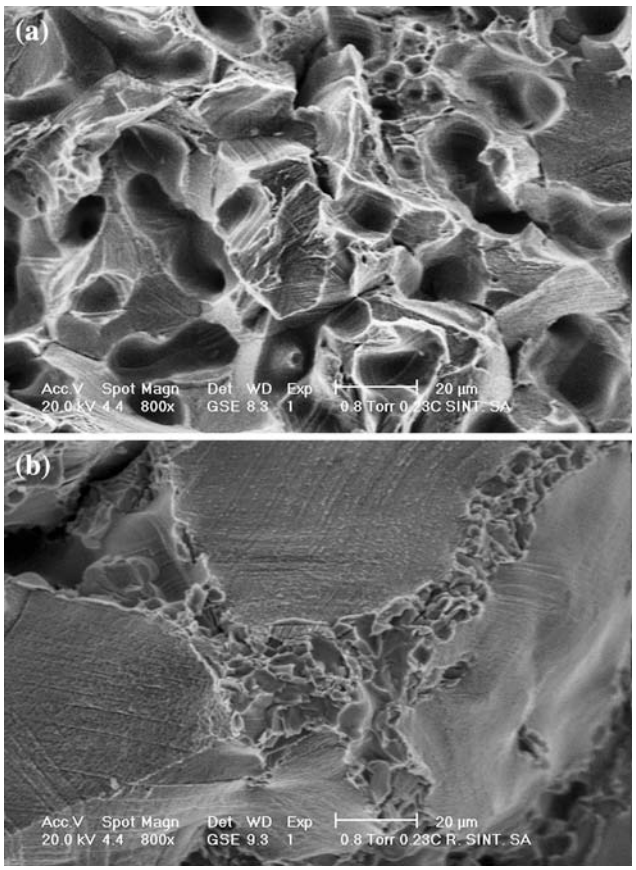

Fig. 9 Fracture surface for the SA materials. **a** LT. **b** HT

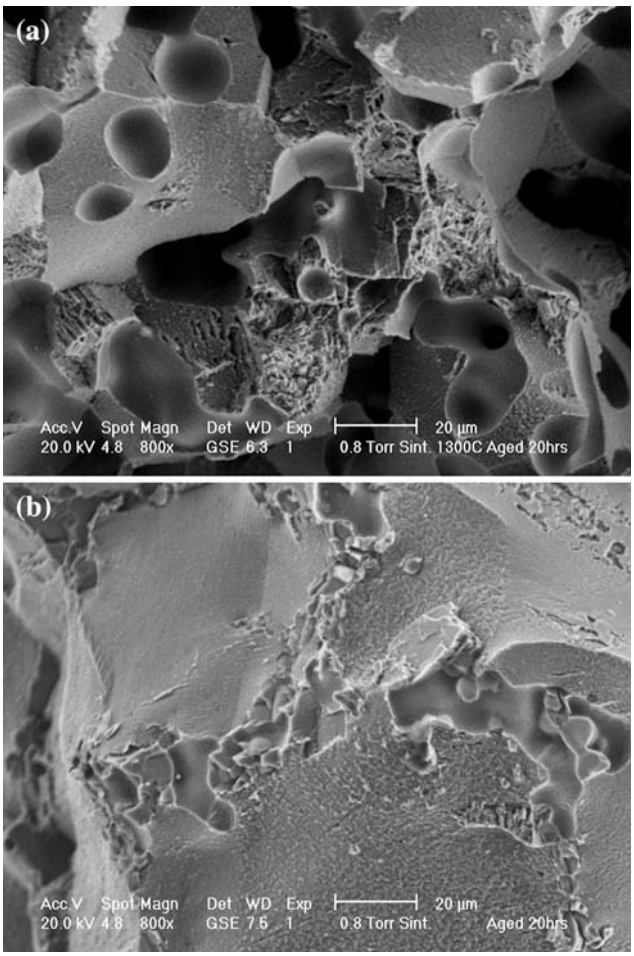

Fig. 10 Fracture surface for the aged materials. **a** LT. **b** HT

precipitation. Fracture is fully intergranular, as shown in Fig. 10.

Because of the more intense precipitation, the materials sintered at higher temperature present a higher YS and UTS than the LT materials, but the ductility is still lower (Table 3).

Tensile properties of the as-sintered and of the solution-annealed materials are characterized by a large difference between YS and UTS, which is representative of a high strain hardenability. Figure 11 shows the true stress–true strain plots. There is an evident deviation from the linear behavior described by the Ludwik–Hollomon equation [21], and the upward curvature is significant of the increasing strain hardenability with plastic strain [13].

It is well known that austenite is metastable in cobalt alloys and transforms into hcp martensite on straining, providing an additional contribution to strain hardenability by the well-known transformation-induced plasticity (TRIP) phenomenon [13, 22]. Kim and Lin [23] proposed a three-parameter model to determine the strain hardening coefficient for a metastable austenite in steel. The correlation between true stress and true strain, assumed to be quadratic, is

$$\ln \sigma = a(\ln \varepsilon)^2 + b(\ln \varepsilon) + c \tag{1}$$

where a, b, and c are constants to be determined by interpolation of experimental data; experimental data show that a linear relationships can be assumed between strain hardening coefficient n and true strain, then the following equation is proposed by Kim and Lim [23]:

$$n = d \ln \sigma / d \ln \varepsilon = M\varepsilon + N \tag{2}$$

where M and N are temperature-dependent constants. Upon integration of Eq. 2, the following flow equation is obtained:

$$\sigma = K\varepsilon^N \exp(M\varepsilon) \tag{3}$$

where K is a constant depending on the material, while M describes how the flow stress increases with the plastic strain because of the strain-induced transformation of austenite.

Figure 12 shows the results of fitting of Eq. 2, and Table 4 lists K, M, and N parameters. The correlation parameter is also included to evaluate the goodness of the model.

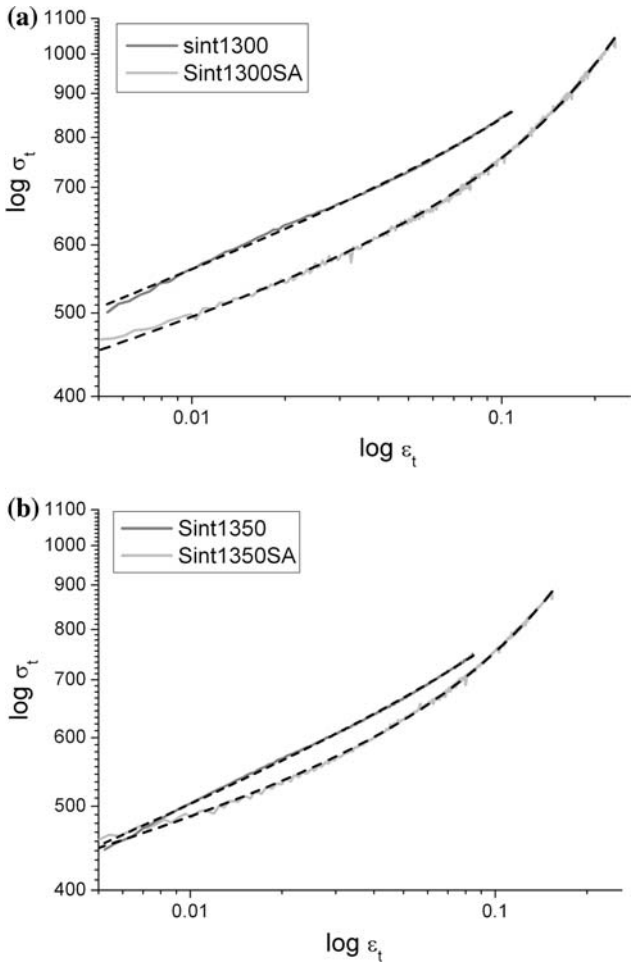

Fig. 11 True stress–true strain plot of the as-sintered and solution-annealed materials

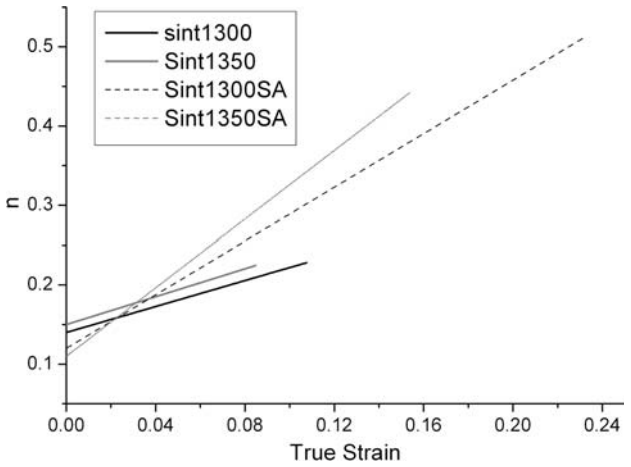

Fig. 12 Strain hardening coefficient versus plastic strain for as-sintered and SA materials

Table 4 Parameters of the fitting of plastic field

Material	*K*	*M*	*N*	R^2
LT				
As sintered	1080.29	0.82	0.14	0.9991
Sintered + SA	839.43	1.69	0.12	0.9992
HT				
As sintered	1012.34	0.88	0.15	0.9993
Sintered + SA	775.29	2.16	0.11	0.9992

N, which represents the initial work hardening coefficient, is quite low in all the materials. The increase in strain hardening with strain is represented by *M*; it is similar between the two as-sintered materials, and is larger in HT than in LT after solution annealing, suggesting a correlation with the amount of martensite.

Discussion

The mechanical properties of the investigated alloys depend mostly on carbides and sigma phase precipitated on sintering at the grain boundaries and within the eutectic cells. These precipitates have a negative effect on ductility since they promote a brittle fracture along the matrix grain boundaries and within the eutectic cells. Mechanical properties are improved by solution annealing, the effectiveness of which depends on the as-sintered microstructure.

The increase in the sintering temperature has a twofold effect: (a) the amount of carbides increases and both tensile strength and ductility decrease consequently and (b) some residual carbides remain at the grain boundary after solution annealing, and the mechanical properties of the LT sintered alloy are still better. The effect of these microstructural characteristics is so strong that it prevails on that density. Indeed, density of the LT-sintered alloy is only 91% of the theoretical one, while that of the HT material approaches 100%.

Aging causes an extensive intragranular carbide precipitation but, at the same time, a grain boundary precipitation of an hcp phase decreases ductility below that of the as-sintered materials.

The presence of secondary precipitates plays a fundamental role in determining tensile properties. Nevertheless, the characteristics of the metallic matrix influence the deformation behavior of the material, which is characterized by a great work hardenability. This characteristic provides some plasticity even in the presence of an intergranular fracture (which, usually, results in a purely brittle behavior).

Plasticity is given by both the inherent defectiveness of the two matrix constituents (fcc austenite and hcp martensite) and the strain-induced martensitic transformations of the fcc austenite.

The cobalt alloy has a low stacking fault energy, which promotes stacking faults formation and twinning [4, 7, 18, 19]. Interaction of dislocations of limited mobility with other sessile dislocations, and with stacking faults and twins, can lead to very high strain hardening rates that produce intensive localized stresses which need to be relieved to allow the material to resist higher loads [4]. This effect gives rise to quite an extensive plasticity even in the presence of a grain boundary surface embrittled by precipitates, as in as-sintered and to some extent in the SA materials. However, in the presence of the additional intragranular Widmanstätten precipitation, as in aged material, strain results mainly localized at the grain boundaries [8] and fracture is preceded by a slight plastic deformation.

The effect of the strain-induced martensitic transformation of austenite was studied by using the model proposed for metastable austenite in stainless steels to determine the strain hardening coefficient and its dependence on plastic strain, as a result of the plastic deformation of austenite and martensite and of the phase transformation. The strain hardening coefficient increases after solution annealing, in particular in the material sintered at high temperature. This material differs from the low temperature one for both presence of some residual carbides at the grain boundary and the higher amount of martensite. Because of the large density of stacking faults which accompany its formation on heat treatment [8], martensite provides an additional contribution to work hardenability.

Conclusions

The microstructure and tensile properties of a 0.23%C Co–Cr–Mo alloy produced by MIM were investigated. The as-sintered microstructures have quite large grain size and contain a significant amount of carbides; the type and quantity of carbides depend on the sintering temperature. The effect of carbides on mechanical properties is so strong that the material with the less amount of carbides has better strength and ductility than that having a higher amount, despite the lower density.

The amount of carbides was almost completely reduced by solution annealing. This leads to an increase in ductility and a decrease of YS. UTS increases with solution annealing, because of the extended ductility. Aging causes the precipitation of both intragranular carbides and grain boundary hcp_1 and hcp_2. The consequence on mechanical properties is negative, since the increase in hardness and YS is accompanied by an excessive reduction of ductility.

In both as-sintered and SA conditions, the material displays a noticeable strain hardenability, which is due to the inherent structural properties of fcc and, more, of hcp phases, and to the TRIP effect.

Acknowledgement The authors are grateful to Ph.D. student Ivan Lonardelli for the XRD analyses.

References

1. Kilner T, Pilliar RM, Weatherly GC, Allibert C (1982) J Biomed Mater Res 16:63
2. Weeton JW, Signorelli RA (1955) Trans Am Soc Met 47:815
3. Caudillo M, Herrera-Trejo M, Castro MR, Ramirez E, Gonzalez CR, Juarez JI (2002) J Biomed Mater Res 59(2):378
4. Mancha H, Gomez M, Castro M, Mendez M, Mendes J, Juarez J (1996) J Mater Synth Process 4(4):217
5. Saldivar Garcia AJ, Lopez HF (2005) J Biomed Mater Res 74A:269
6. Dobbs HS, Robertson JLM (1983) J Mater Sci 18:391. doi: 10.1007/BF00560627
7. Taylor RNJ, Waterhouse RB (1983) J Mater Sci 18:3265. doi: 10.1007/BF00544151
8. Vander Sande JB, Coke JR, Wulff J (1976) Metall Trans 7A:389
9. Billiet RT, Billiet TH (2006) A practical guide to metal and ceramic injection moulding. Elsevier, Oxford
10. Johnson JL, Heaney DF. Advanced Powder Products, Inc. www.advancedpowderproducts.com/publications.asp. Accessed 15 March 2009
11. Tandon R (1999) In: Disegi JA, Kennedy RL, Pilliar R (eds) Cobalt-base alloys for biomedical applications, ASTM STP 1365. ASTM, West Conshohocken, p 3
12. Sago JA, Chen H, Broadley MW, Eckert JK (2009) Adv Powder Metall Part Mater 4:111
13. Muterlle PV, D'Incau M, Perina M, Bardini R, Molinari A (2008) Adv Powder Metall Part Mater 4:183
14. Lutterotti L, Matthies S, Wenk HR, Shultz AS, Richardson JW (1997) J Appl Phys 81:594
15. Lonardelli I, Wenk HR, Lutterotti L, Goodwin M (2005) J Synchrotron Radiat 12:354
16. Clemow AJT, Daniell BL (1979) J Biomed Mater Res 13:265
17. Shortsleeve FJ, Nicholson ME (1951) Trans Am Soc Met 43:142
18. Rajan K (1982) Metall Trans 13A:1161
19. Rajan K (1984) Metall Trans 15A:1335
20. Betteridge W (1982) Cobalt and its alloys. Ellis Horwood, Chichester
21. Dieter GE (1988) Mechanical metallurgy (adapted by D. Bacon), SI Metric edn. Materials Science & Metallurgy, Singapore
22. Salinas-Rodriguez A, Rodriguez-Galicia JL (1996) J Biomed Mater Res 31:409
23. Kim YG, Lim CY (1988) Metall Trans 19A:1625